A Biophysically-Based Framework for the Simulation and Visualization of Chlorophyll Fluorescence Under Different Illumination Conditions

by

Frank Fan

A thesis
presented to the University of Waterloo
in fulfillment of the
thesis requirement for the degree of
Master of Mathematics
in
Computer Science

Waterloo, Ontario, Canada, 2026

Author's Declaration

I hereby declare that I am the sole author of this thesis. This is a true copy of the thesis, including any required final revisions, as accepted by my examiners.

I understand that my thesis may be made electronically available to the public.

Abstract

Chlorophyll is the most important pigment for the sustainability of life on the planet. Its light absorbing properties, besides being directly associated with the green colouration of plants, play a key role in the photosynthesis process. These properties can also elicit fluorescence, a complex phenomenon leading to striking material appearance changes. Accordingly, its predictive simulation can strengthen the fidelity of realistic image synthesis frameworks, notably those targeting chlorophyll-containing materials. Moreover, the systematic visualization of chlorophyll fluorescence can lend itself to interdisciplinary applications in related areas such as botany, ecology, remote sensing and photonics. Despite these aspects, chlorophyll fluorescence remains relatively overlooked in the computer graphics literature, with related works accounting for it as a complementary rendering component tied to visible light stimulus. In this thesis, we introduce a biophysically-based framework for the simulation and visualization of the chlorophyll fluorescence elicited by light excitation in the ultraviolet and visible spectral domains. It employs an algorithmic approach, centered on the use of fluorescence spectroscopy principles, that can be used in the rendering and investigation of other fluorescent materials. We assess the proposed framework's predictive capabilities through the rendering of images depicting fundamental qualitative traits verified in actual observations of chlorophyll fluorescence. We also demonstrate its effectiveness and applicability in realistic image synthesis through sequences of images depicting chlorophyll solutions under various experimental characterizations and illumination conditions.

Acknowledgements

First and foremost, I would like to thank my supervisor, Gladimir Baranoski, for his guidance, wisdom, and most importantly, his belief in me. I am deeply grateful for the kindness, patience, and understanding that he has shown. The growth I have experienced as both a researcher and a person is a direct result of his faith and trust in me.

I would also like to thank Professor Paulo Alencar and Professor Toshiya Hachisuka for taking the time to review my thesis and for providing invaluable feedback.

This journey would not have been the same without the members of the Natural Phenomena Simulation Group: Petri, Francis, and Scott. I am grateful to have had them as labmates, and even more so as friends. The experiences and memories that we have shared will last a lifetime and be remembered fondly.

I would also like to thank my partner, Caryn, for her encouragement and understanding throughout this process. She always kept me grounded and I sincerely appreciate her unconditional support along this endeavour.

Finally, words cannot even begin to express the level of gratitude I have for my parents and their endless belief and support. They have instilled in me the confidence to pursue whatever I set my mind to and have gone above and beyond to provide me opportunities to do so. This thesis stands as a testament to their unwavering love.

Dedication

Dedicated to my parents, Fan Qingzhuo (范庆卓) and Zhang Xiaoli (张小丽).

Table of Contents

List of Figures

List of Symbols

N Avogadro number. $N = 6.06 \times 10^{23}\ mol^{-1}$. 19

Q Quantum yield. 15, 16

R Gas constant per gram molecule. $R = 8.315 \times 10^{7}\, erg\, K^{-1}\, mol^{-1}$. 19

A Absorbance. 20

μ_a Absorption coefficient. $\left[\frac{1}{m}\right]$ 17

σ_a Probability that the attenuation event is absorption. 17

μ Attenuation coefficient. $\left[\frac{1}{m}\right]$ 17

β Isothermal compressibility. $\beta = 4.95 \times 10^{-11}\, cm^2\, dyne^{-1}$. 19

c Concentration. $[M]$ 20

d The distance from the attenuation point to the boundary of the medium. $[m]$ 14–17

ε Molar extinction coefficient. $\left[\frac{L}{cm \cdot mol}\right]$ 20

η Index of refraction. 19

κ Extinction coefficient of liquid water. 21

A_m Measured absorbance. 21

c_m Considered concentration. $[M]$ 21

ε_m Measured molar extinction coefficient. $\left[\frac{L}{cm \cdot mol}\right]$ 21

l_m Considered optical path length. $[cm]$ 21

l Optical path length. $[m]$ 20

ϕ_R Azimuthal angle of the scattered light. $[rad]$ 19

p The distance that a ray travels in a medium before interacting with a particle. $[m]$ 14–18

ξ A random variable used in the stochastic process. 15, 16, 18, 19

$\vec{r}$ A primary ray used in a path tracing or other ray tracing algorithm. 17

μ_s Scattering coefficient. $\left[\frac{1}{m}\right]$ 17, 19

σ_s Probability that the attenuation event is scattering. 17

τ Optical thickness depth. $[cm]$ 18

$\mathcal{T}$ Absolute temperature. $[K]$ 19

θ_R Polar angle of the scattered light. $[rad]$ 19

T Transmittance. 18, 20

λ Wavelength. $[nm]$ 18, 19

x Attenuation point where an incident ray strikes a medium particle. 17

Chapter 1

Introduction

The modelling of material appearance remains an important research topic in computer graphics. In particular, it plays a central role in the high-fidelity rendering of natural scenes composed of organic and inorganic materials. The realistic depiction of these materials involves the simulation of light absorption and scattering processes directly responsible for their appearance attributes (*e.g.*, colour and translucency) [13].

In general, the simulation of these processes is carried out assuming the decoupling of energies associated with different light wavelengths. More precisely, the energy of light interacting with a material at a certain wavelength is independent of the energy at another wavelength [16]. There are materials, however, capable of absorbing light at a given wavelength and re-emitting it at another (usually longer) wavelength, a phenomenon known as *fluorescence* [28].

This phenomenon may markedly change a material's appearance when observed under certain illumination conditions (Fig. 1.1). It can also affect the light interactions with the surrounding environment. These aspects make the predictive simulation of fluorescence

relevant for realistic image synthesis [19]. However, despite the recent advances in this area, this phenomenon is still relatively overlooked in the computer graphics literature, notably with respect to organic materials.

Chlorophyll is a ubiquitous organic pigment that actively participates in the process of photosynthesis and gives plants their green colour by absorbing impinging light. A significant portion of the absorbed light is transformed into chemical energy, while the remaining energy may be re-emitted through fluorescence [24]. Due to its scientific importance (*e.g.*, it can serve as an indicator of vegetation productivity [26] and stress [41]) chlorophyll fluorescence has been extensively investigated in the scientific literature.

In computer graphics, to the best of our knowledge, the simulation of chlorophyll fluorescence has mainly been considered with respect to the rendering of believable images of ocean waters [8, 22, 23], with the phenomenon being elicited by visible light. We also note that existing works depicting fluorescent materials observed under ultraviolet (UV) light [3, 4, 27, 34, 50] do not explicitly examine chlorophyll and its specific light emission capabilities in this spectral domain.

In this thesis, we propose a predictive, biophysically-based framework for the simulation and visualization of chlorophyll fluorescence elicited by independent or simultaneous exposure to ultraviolet and visible light. We comprehensively assess the fidelity [20] of its predictions through the rendering of images depicting fundamental qualitative traits verified in actual observations of this phenomenon. We also showcase its effectiveness and applicability in realistic image synthesis [19] through sequences of images generated considering distinct material characteristics and different illumination conditions.

In short, the main contributions of this work are three-fold. It presents a framework that can enable the generation of images that are not only realistic depictions of chlorophyll

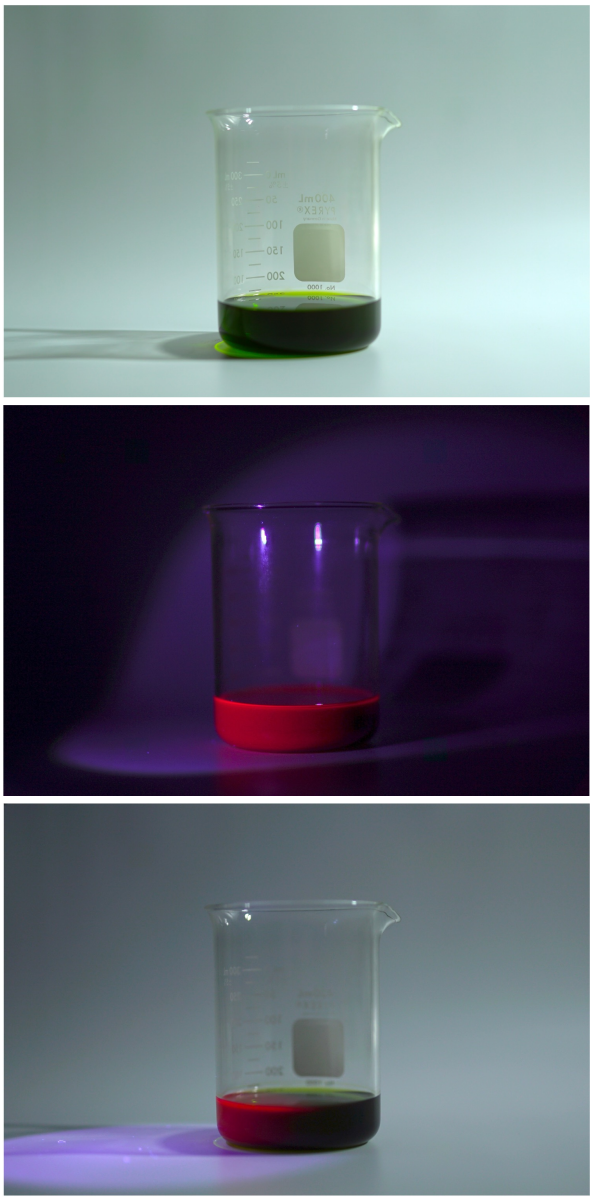

Figure 1.1: Photographs illustrating the appearance of a chlorophyll solution under different illumination conditions. Top: green colour elicited by visible light exposure. Middle: red (fluorescent) colour elicited by ultraviolet light exposure. Bottom: Mixed colours elicited by the simultaneous ultraviolet and visible light exposure.

fluorescence, but are also controlled by biophysically meaningful parameters and less dependent on manual tweaks. Moreover, we note that chlorophyll fluorescence can be found in a wide range of lifeforms, from higher plants to algae and moss [59]. Accordingly, the proposed framework provides a sound basis for the effective incorporation of chlorophyll fluorescence into comprehensive material appearance models designed for these lifeforms. Lastly, the proposed framework and data gathered for its development and evaluation also offer an *in silico* platform for the testing of hypotheses involving this fundamental phenomenon. This, in turn, may also contribute to knowledge advances in other fields such as botany, ecology, remote sensing and photonics, just to name a few.

The remainder of this thesis is organized as follows. In Chapter 2, we briefly review relevant aspects and terminology associated with chlorophyll fluorescence. In Chapter 3, we concisely examine related computer graphics works involving this phenomenon and rendering methods employed in its visualization. We then present the proposed framework in Chapter 4. In Chapter 5, we assess its predictive capabilities and applicability to realistic image synthesis. Finally, in Chapter 6, we conclude the thesis and indicate directions for future work in this area.

Chapter 2

Biophysical Background

In this chapter, we provide a concise overview of the biophysical concepts relevant to the development of the proposed framework. In Section 2.1, we briefly describe the phenomenon of fluorescence and its related terminology. In Section 2.2, we further detail how fluorescence is elicited by chlorophyll molecules. Readers interested in more information are encouraged to examine comprehensive publications on these topics, such as the works by Lakowicz *et al.* [39] on fluorescence spectroscopy or by Hall and Rao [24] on photosynthesis, employed as supporting references in this thesis.

2.1 Fluorescence Terminology

Luminescence can be described as a material's light emission caused by the return of its excited (by an external stimulus) electrons to their ground state (relaxation) [39]. Fluorescence, in turn, is a form of luminescence where the mechanism of electron excitation corresponds to the absorption of photons [65] and the emission of light occurs within 10^{-8} s

[21], which, to the naked human eye, can be considered instantaneous. When fluorophores (molecules of a fluorescent material) are photonically excited, they jump from their neutral, ground state to an excited state [39] (Fig. 2.1). At relaxation, they return to the ground state and energy may be released through the emission of a photon.

The absorption spectrum of a fluorophore describes the fraction of incident wavelengths of electromagnetic radiation that the material absorbs. The excitation spectrum depicts the relative fluorescence intensity (for a fixed emission wavelength) produced by a range of (excitation) wavelengths [65]. Its emission spectrum, on the other hand, represents the relative fluorescence intensity for a fixed excitation wavelength [65].

For most fluorophores, the emission spectrum (or fluorescence spectrum [17]) is considered independent of the excitation spectrum. We also note that the absorption and excitation spectra generally peak at the same wavelength and, for practical purposes, the former can be used to represent the latter [39].

A fluorophore's quantum yield (sometimes referred to as quantum efficiency [21]) is defined as the ratio between the number of emitted photons relative to the number of absorbed photons [39, 65]. It is worth noting that the quantum yield of a fluorophore is also independent of excitation wavelength [39].

2.2 Chlorophyll Fluorescence

There are four major types of chlorophyll: *a*, *b*, *c* and *d* [67]. Under *in vivo* conditions, they are embedded in pigment-protein-lipid complexes present in photosynthetically active cells (*e.g.*, found in plant leaves) [59]. The reader interested in more details about the photosynthetic and energy conversion processes is referred to Appendix A. While the blue-

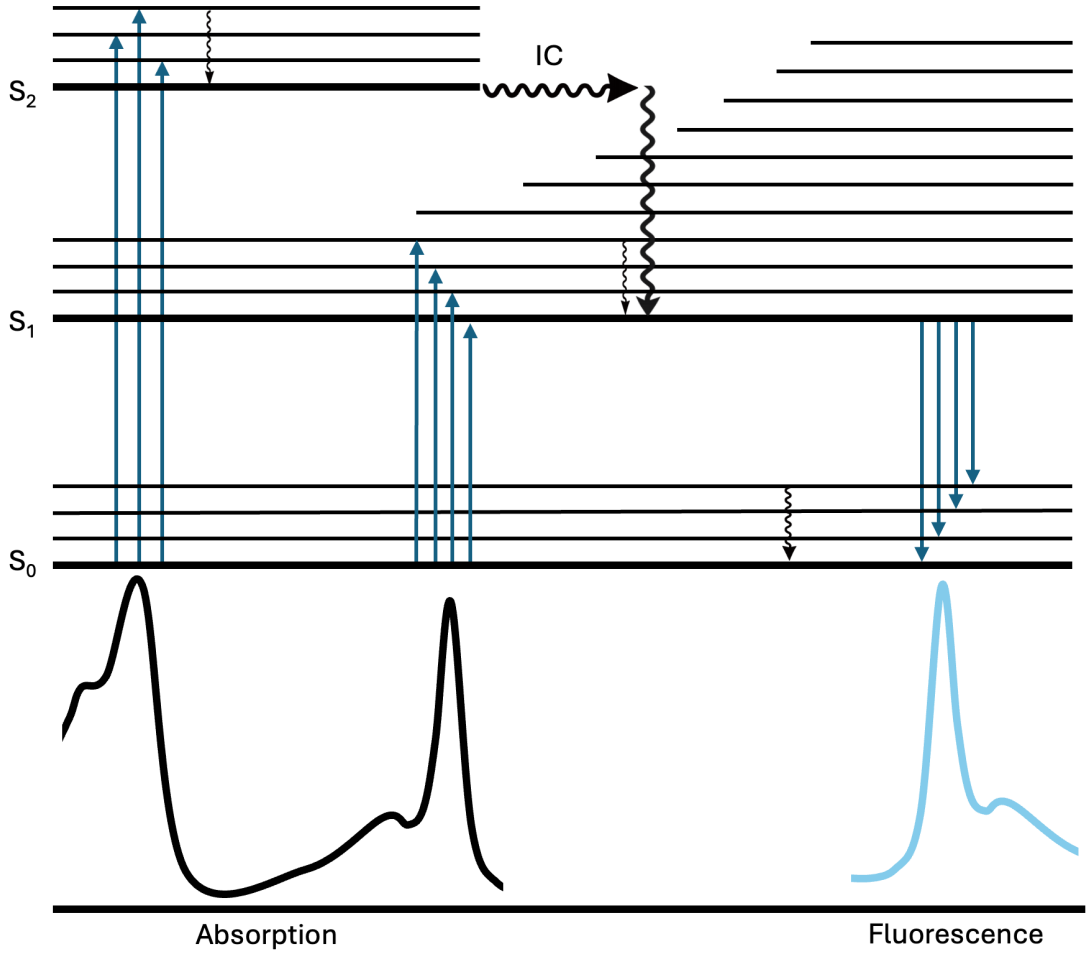

Figure 2.1: A Jablonski [30] diagram of relative positions of chlorophyll's absorption and fluorescence spectra. S_0 represents the ground state of a molecule of chlorophyll, while S_1 and S_2 represent the first two excited states of a fluorophore [39]. IC stands for internal conversion [65] and it represents a nonradiative transition between S_1 and S_2.

green chlorophyll a is present in all oxygen-photosynthetic organisms [24], yellow-green chlorophyll b is present in leaves of higher plants and in green algae [24]. Chlorophylls c and d, on the other hand, can be found in brown and red algae, respectively [24]. In this work, without loss of generality, we focus on chlorophyll a fluorescence. This choice was motivated by the prominent occurrence of this type of chlorophyll [59] and the larger availability of supporting empirical information in comparison with the other types [24].

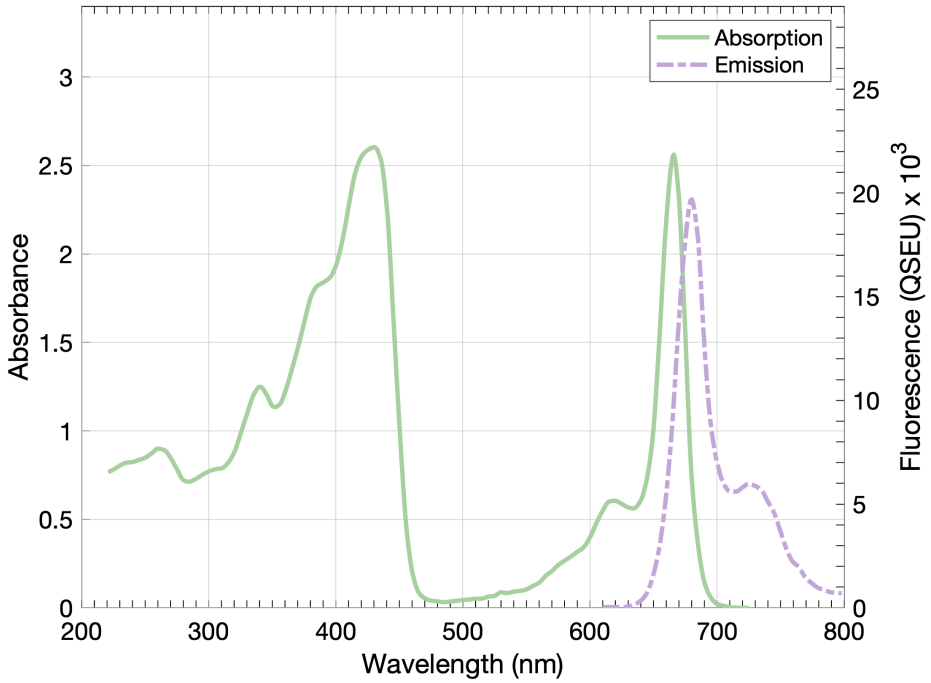

Figure 2.2: Absorption and emission spectra of chlorophyll a [9]. The chosen concentration was 150 μM. The emission spectrum was measured at an excitation wavelength of 355 nm, and it is displayed in units of QSEU (quinine sulphate equivalent units, with quinine sulphate being a fluorescence standard reference material used when comparing emission spectrums [66]).

The absorption spectrum of chlorophyll a is comprised of two peaks in the blue and red spectral regions (Fig. 2.2). Thus, when a chlorophyll solution (*e.g.*, obtained by immersing a plant leaf in alcohol) is illuminated by a visible light source, photons near these peaks are more likely to be absorbed than those in the green region.

The absorption of a "blue" photon (a photon travelling in the short wavelength region of the visible spectrum) excites the chlorophyll molecule to the excited state of S_2, while that of a "red" photon (a photon travelling in the long wavelength region of the visible spectrum) will excite it to S_1 [24] (Fig. 2.1). Due to the instability of the excited molecule, electrons rapidly return to the ground level and, in turn, release the absorbed photon's energy [24]. This release of excitation energy is mainly used to drive photochemical reactions that initiate the photosynthetic energy conversion [38]. Excess energy is either released as thermal dissipation or emitted as a photon of lower energy (longer wavelength) [24, 38]. Chlorophyll fluorescence emission only occurs in the red region due to the fact that decay of excitation between excited states takes place within 10^{-13}s of absorption, while fluorescence emission requires about 10^{-9}s [24]. Therefore, chlorophyll fluorescence occurs in the red region regardless of the absorbed light's wavelength [24].

However, when an ultraviolet light source is employed, the non-absorbed photons cannot be detected by the human eye since they are outside the visible spectral domain. This results in a perception of red fluorescence stronger than that elicited by visible light [24]. In the former case, the non-absorbed rays are detected by the human eye, contributing to a broader colour perception (associated with both green and red wavelengths). It is important to note that absorption and fluorescent emission are separate processes [64].

Lastly, it is also worth mentioning that the quantum yield of chlorophlyl under *in vitro* conditions is significantly higher than that verified under *in vivo* conditions [14, 45]. Therefore, the fluorescence of a chlorophyll solution is much stronger and more noticeable

than that of a plant organ (e.g., a leaf).

2.3 Inelastic Phenomena

Scattering events result in the perturbation of the direction of propagation of light traversing a medium (or material). When this perturbation is accompanied by a change of wavelength, these events are termed inelastic [5]. Otherwise, they are classified as elastic.

Similarly, fluorescence can be described as an inelastic phenomenon since it results from an attenuation event accompanied by a wavelength change. More specifically, light is re-emitted at a longer wavelength (lower energy) than that of the excitation (traversing) light [39].

Chapter 3

Related Work

The simulation of fluorescence involving inorganic materials has been extensively examined in the field of computer graphics. Since a comprehensive review of this topic is beyond the scope of this thesis, the interested reader is referred to representative works in this area such as those by Glassner [15], Wilkie *et al.* [70], Hullin *et al.* [27] and Jung *et al.* [34]. For conciseness, in this chapter, we focus on computer graphics works that have specifically involved the simulation of fluorescence produced by chlorophyll or chlorophyll containing organisms [8, 22, 23].

Cerezo and Seron [8] extended the radiative transfer equation[1] to consider inelastic volumetric processes. To showcase their system, they produced renderings of natural waters which took into account fluorescence from chlorophyll *a*. More specifically, they investigated the simulation of ocean waters with a high concentration of this pigment, and utilized measured absorption data [48] to characterize their seawater volume. Furthermore, they

[1]The radiative transfer equation describes the change in radiance travelling along a certain direction at a certain point in a differential volume element [10].

noted that the distribution of the chlorophyll a fluorescence emission wavelengths is centered around 685 nm. They also stated that even though the exciting wavelength does not affect the emission wavelength, it affects the strength of the fluorescence signal. Accordingly, they approximated the fluorescence emission spectrum with a Gaussian function provided by Mobley [48]:

$$h_p(\lambda) = \frac{1}{\sqrt{2\pi}\lambda_\sigma} \exp\left[-\frac{(\lambda - \lambda_0)^2}{2\lambda_\sigma^2}\right], \tag{3.1}$$

where $h_p(\lambda)$ is the chlorophyll fluorescence emission wavelength function, λ_0 is the wavelength of maximum emission (which, in the case of chlorophyll a fluorescence, is reportedly to be 685 nm [48]) and $\lambda_\sigma = 10.6\ nm$ is the standard deviation of the Gaussian (Fig. 3.1).

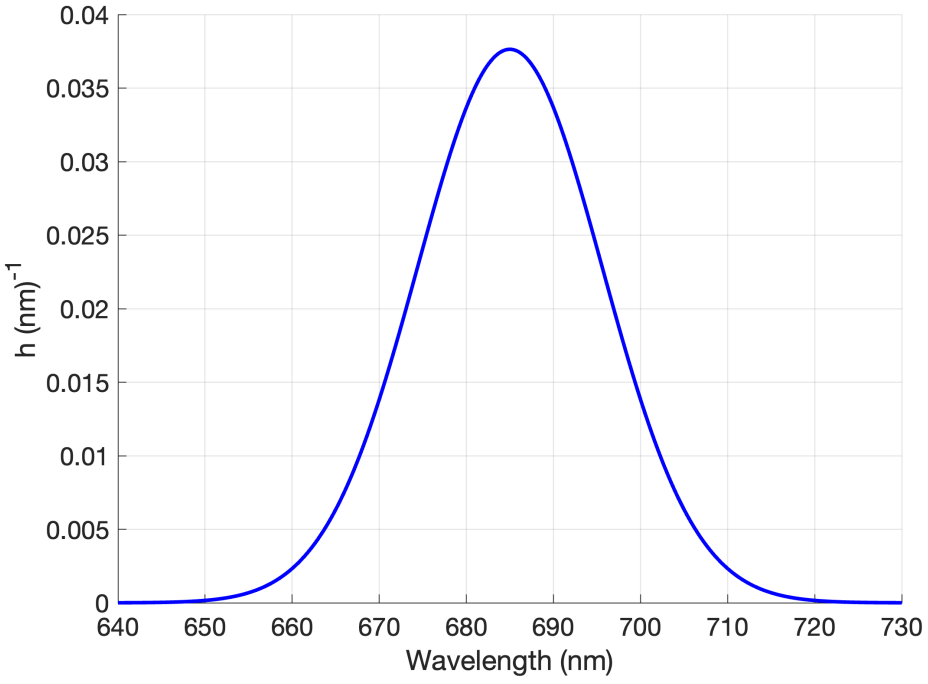

Figure 3.1: Graph depicting an approximation (Eq. 3.1) of chlorophyll a's fluorescence emission spectrum. Redrawn from Mobley [48].

Cerezo and Seron [8] qualitatively compared scenes depicting both elastic and inelastic scattering phenomena (*i.e.*, fluorescence) and scenes depicting only the former. They reported that there were no visible differences. Quantitatively, they observed that the net absorbed energy in the elastic case was always greater than that of the inelastic case except in the region near 680 nm. According to them, the emitted absorbed energy (through fluorescence) was reabsorbed, mitigating the difference between the two cases in that region.

Gutierrez *et al.* [22] also investigated the simulation of inelastic scattering events in their non-linear volume extension of the photon mapping algorithm [33]. They employed a Russian roulette algorithm [25] in their fluorescence simulation, utilizing reported data and various sampling techniques. They then incorporated their simulation in the rendering of ocean waters as a case study. They considered two main seawater cases: one with varying concentrations of chlorophyll (with this pigment mainly absorbing visible light at wavelengths outside the blue region of this spectral domain) and another with a high concentration of dissolved organic matter (or yellow matter). Similar to Cerezo and Seron [8], Gutierrez *et al.* [22] qualitatively compared different images of simulated ocean water characterized by varying parameters.

Later, in their bio-optical model for the visualization of underwater ocean optics that expands on the previously mentioned work [22], Gutierrez *et al.* [23] included the components of yellow matter, chlorophyll-containing phytoplankton and minerals. However, they noted that they only considered incident wavelengths in the range of 370 to 690 nm, and reported that only those wavelengths could trigger fluorescence.

Lastly, Jarabo and Arellano [32], in their implementation of bidirectional rendering of vector light transport, made use of the chlorophyll material (and its respective properties) from Gutierrez *et al.* [23]. They used a time-resolved render to showcase the red emission of absorbed photons after the excitation source emitting visible light was turned off.

Chapter 4

Proposed Framework

In this chapter, we describe the framework proposed for the biophysically-based simulation of chlorophyll fluorescence. It employs an algorithmic formulation centered on the use of stochastic techniques [25] and geometrical (ray) optics concepts [18]. Fig. 4.1 provides a high-level overview of the decision tree that a light ray (originating from a virtual camera) undergoes when interacting with the material (chlorophyll solution).

After the incident (camera) ray intersects with the volume representing the solution, we compute its path length (Section 4.1), denoted by p_i, *i.e.*, the distance that the ray travels before interacting with a chlorophyll molecule. If p_i is greater than the distance, d_1, to the volume boundary, the ray is transmitted. Otherwise, it is deemed to be attenuated by an elastic scattering event or an absorption event, which are determined probabilistically.

In the case of an elastic scattering event, we perturb the ray's direction of propagation (Section 4.1.1) and continue to trace its path. In the case of an absorption event (Section 4.1.2), we check the ray's wavelength. If it is not within the chlorophyll's emission spectrum domain, we terminate its path. Otherwise, we determine if it is associated with

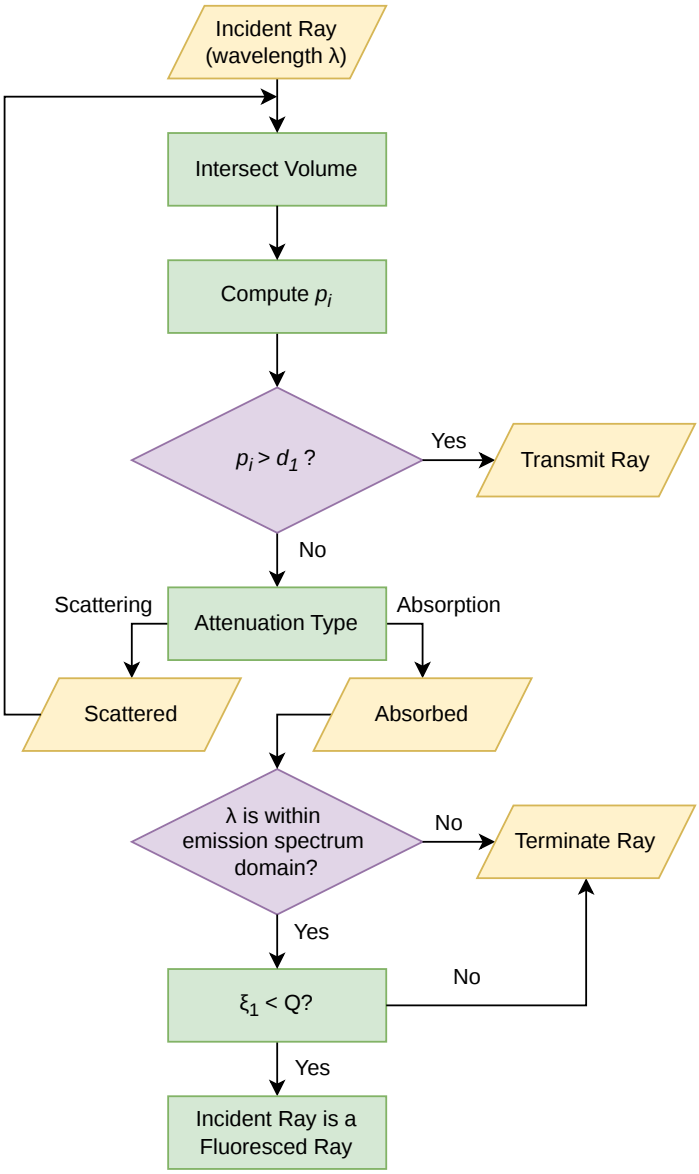

Figure 4.1: Flowchart depicting the decision tree that a camera (incident) ray undertakes before determining that it is a fluoresced ray. The parameters p_i, d_1, Q and ξ_1 correspond to the ray's path length, the distance to the volume boundary, the quantum yield and a random number uniformly distributed in [0,1), respectively.

a fluorescence event as follows.

Recall that the quantum yield, Q, represents the ratio between the number of emitted photons relative to the number of absorbed photons [39, 65]. Thus, we generate a random number ξ_1, uniformly distributed in [0,1). If $\xi_1 < Q$, the ray's absorption is deemed to be linked to a fluorescence event, *i.e.*, the incident ray is deemed to be a fluoresced ray. Otherwise, the ray's path is terminated.

Once it is determined that a fluorescence event has occurred, we proceed to trace the corresponding excitation ray. More specifically, we generate a ray from the point of attenuation to a sample point on a randomly selected light source present in the scene. Note that that this excitation ray is associated with a wavelength shorter than that of the original incident ray, and it is within the spectral power distribution of the selected light source.

We then compute the excitation ray's path length (Section 4.1), denoted by p_e, to determine whether the fluoresced ray should be terminated or traced to the light source (Fig. 4.2). More precisely, if p_e does not exceed the distance, d_2, to the volume boundary, the excitation ray is not generated and the corresponding fluoresced ray's path is terminated. Otherwise, the excitation ray is generated from the attenuation point and the fluoresced ray's path is traced to the light source.

4.1 Attenuation

We remark that the attenuation of light propagating in a material, or medium, can occur through absorption and scattering events. These, in turn, depend on the material's absorption and scattering coefficients [29] denoted by μ_a and μ_s, respectively. Their sum

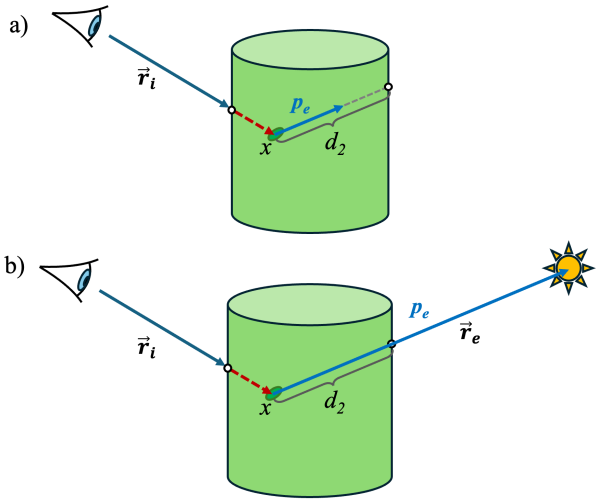

Figure 4.2: Diagrams illustrating the handling of a fluoresced ray, $\vec{r_i}$, and the corresponding excitation ray, $\vec{r_e}$. (a) If the path length, p_e, does not exceed the distance, d_2, to the volume boundary, the fluoresced ray's path is terminated. (b) Otherwise, the excitation ray is deemed to have reached the attenuation point, x.

gives the attenuation coefficient, denoted by μ. These coefficients are typically measured in inverse length units [58].

Given the occurrence of an attenuation event, the probability of absorption is given by:

$$\sigma_a = \frac{\mu_a}{\mu}. \tag{4.1}$$

Similarly, the probability of scattering is given by:

$$\sigma_s = \frac{\mu_s}{\mu}. \tag{4.2}$$

Considering a homogeneous medium, the attenuation coefficient is spatially invariant. Thus, the optical thickness depth τ is linearly proportional to the distance d along the ray

[58]:

$$\tau = d\,\mu, \tag{4.3}$$

such that the transmittance (transmitted to incident light flux[1], or power, ratio [47]) T can be expressed as:

$$T = e^{-\tau}. \tag{4.4}$$

It follows that the free path length p can be computed as [58]:

$$p(\xi_2) = -\frac{1}{\mu(\lambda)} \ln(\xi_2), \tag{4.5}$$

where ξ_2 is a random number uniformly distributed in [0,1).

4.1.1 Scattering

For practical purposes, one can consider the scattering behaviour of an alcoholic solution of chlorophyll similar to that of liquid water, particularly considering alcohol solvents whose optical properties (*e.g*, refractive indices and Rayleigh ratios[2]) closely align with those of water [1, 54, 56]. Although any amount of scattering would be relatively small, we include a wavelength-based scattering coefficient for completeness and approximate it

[1]Flux, or radiant power (commonly referred to as *power*), refers to the total amount of radiant energy passing through a surface per unit time, measured in watts (W or J s^{-1}) [61]. Radiant energy is a fundamental quantity representing the energy measured in a group of photons (rays) and has units in joules (J) [61].

[2]According to Kerker [36], the Rayleigh ratio, R_θ, is defined as the intensity of scattered light in the direction θ per unit solid angle [15] and unit scattering volume, normalized by the incident irradiance [15]. The Rayleigh scattering coefficient may be found by integrating the Rayleigh ratio over all solid angles. That is, $\mu_s = \frac{16\pi}{3} R_\theta$ [36].

using measured data for liquid water [12]:

$$\mu_s(\lambda) = \frac{\pi^2}{18}\left(\frac{\beta R \mathcal{T}}{N\lambda^4}\right)(\eta^2-1)^2(\eta^2+2)^2, \tag{4.6}$$

where η is the refractive index of water, λ is the incident wavelength, $\mathcal{T}$ is the absolute temperature (in K units), $R = 8.315 \times 10^7\, erg\, K^{-1}\, mol^{-1}$ is the gas constant, $N = 6.06 \times 10^{23}\ mol^{-1}$ is the Avogadro number, and $\beta = 4.95 \times 10^{-11}\, cm^2\, dyne^{-1}$ is the isothermal compressibility.

For consistency with seminal works [11, 12, 62] on scattering events occurring in water and other homogeneous media whose main scatterers are molecules much smaller than the wavelength of light, the ray direction of propagation is perturbed considering the Rayleigh scattering distribution [46]. Accordingly, the polar perturbation angle θ_R is generated using Algorithm 1, where ξ_3 and ξ_4 are random numbers uniformly sampled from [0,1). As for the azimuthal perturbation ϕ_R, it is symmetrically distributed over [0, 2π), *i.e.*, $\phi_R = 2\pi\xi_5$, where ξ_5 is also a random number uniformly sampled from [0,1). These two angles characterize the direction of scattering (Fig. 4.3).

Algorithm 1: Rayleigh Perturbation

repeat

$\xi_3, \xi_4 \leftarrow \text{random}[0, 1)$

$\theta_R \leftarrow \pi\xi_3$

until $\xi_4 \leq \left(\frac{3\sqrt{6}}{8}\right)(1+\cos^2\theta_R)\sin\theta_R$

return θ_R

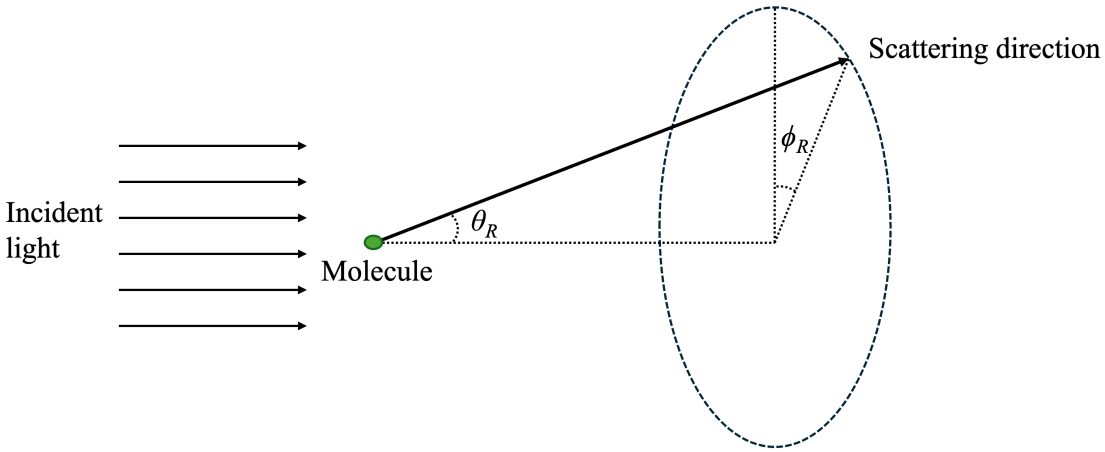

Figure 4.3: Diagram describing a scattering direction represented by a polar angle θ_R and azimuthal angle ϕ_R.

4.1.2 Absorption

Absorbance, A (also known as *optical density*), is the parameter that describes the amount of light that is absorbed and converted to other forms of energy such as heat [47]. It is defined as the logarithm to base 10 of the reciprocal of transmittance [43, 47],

$$A = \log_{10}\left(\frac{1}{T}\right). \tag{4.7}$$

Furthermore, according to the Beer-Lambert law [43], the transmittance of an absorptive material can be expressed as:

$$T = e^{-\varepsilon\, c\, l}, \tag{4.8}$$

where ε and c are the molar absorption coefficient and the concentration of the material, respectively, and l is the optical path length.

Utilizing Eq. 4.7 and Eq. 4.8, the molar extinction coefficient (given in units $\frac{L}{\text{cm}\cdot M}$) can be expressed as:

$$\varepsilon = \frac{A \ln(10)}{c\, l}. \tag{4.9}$$

Thus, in order to obtain the molar extinction coefficient for chlorophyll, one can use Eq. 4.9 and measured absorbance data such that:

$$\varepsilon_{chl}(\lambda) = \frac{A_m(\lambda) \ln(10)}{c_m\, l_m}, \tag{4.10}$$

where A_m is the measured absorbance data, while c_m and l_m respectively represent the concentration and optical path length values considered in the absorbance measurements.

The total (effective) absorption coefficient of a given solution corresponds to the sum of the absorption coefficients of its constituent materials [31]. These, in turn, are obtained by multiplying each material's specific absorption coefficient (s.a.c.) by their corresponding concentration in the solution. Note that the absorption coefficient of liquid water corresponds to its s.a.c. [2]. This, in turn, can be used to approximate the absorption coefficient of an alcoholic (liquid) solvent, such as methanol [52], with optical properties markedly similar to those of water [1, 54, 56]. Accordingly, the absorption coefficient of a chlorophyll solution, with concentration c_{chl} (given units of M) and molar extinction coefficient ε_{chl}, can be calculated as:

$$\mu_a(\lambda) = \zeta_{water}(\lambda) + \varepsilon_{chl}(\lambda)\, c_{chl}, \tag{4.11}$$

where ζ_{water} refers to the s.a.c. of liquid water (given in units of $\frac{1}{cm}$) and it is expressed as:

$$\zeta_{water}(\lambda) = \frac{\kappa(\lambda)\, 4\pi}{\lambda}, \tag{4.12}$$

with $\kappa(\lambda)$ representing the extinction coefficient of liquid water [44, 57].

4.1.3 Emission Approximation

We remark that fluorescence can be described as the emission of a photon at a longer wavelength than that of the corresponding absorbed photon [39]. This involves a numerical shift, also known as the Stokes shift [63], between the incident and emitted wavelength.

It follows that the emission spectrum of a fluorescent material loosely mirrors its absorption spectrum where photons excite molecules from the ground state to the first excited state. This resemblance is known as the "*mirror-image rule*" [21, 39, 65]. In the case of chlorophyll, its emission spectrum mirrors the region around its absorption peak located in the red range of the visible spectrum. We employ this principle to approximate the emission spectrum of chlorophyll. We mirror its absorption spectrum [9] about the vertical line at 673 nm, and then normalize it such that the integral is equal to one. We also note that the emission is isotropic and its direction is independent of the incident direction [39]. It is worth mentioning that we elected to use this approach since measured emission datasets are still scarce in the literature and they are often tied to a specific excitation wavelength.

4.2 Implementation Aspects

The implementation of the proposed methodology can be seen as a new (fluorescent) material class definition for a typical path tracing [16] renderer. Accordingly, as a ray traversing the target material undergoes distinct attenuation events, their effects are cumulatively accounted for in the estimation of the ray's contribution to the radiance[3] (colour) of its

[3]The radiance at a certain point on a surface (or volume) is the reflected quantity that closely approximates the colour of the material (or medium) and it provides an indication of surface (or volume) brightness [61]. It is independent of surface area, the size of the object being inspected and the distance to the observer.

associated pixel. The reader interested in more details about the implementation of the proposed framework is referred to Appendix B.

Chapter 5

Results and Discussion

In this chapter, we assess the predictive capabilities of the proposed framework. We begin with a concise presentation of key components of our *in silico* experimental scenarios. This is followed by a qualitative examination of results obtained for baseline cases, which were selected to enable the verification of distinct features and trends observed in actual experiments involving chlorophyll solutions. Lastly, we further showcase the effectiveness and applicability of the proposed framework by exploring scenes with more complex light exposure conditions.

5.1 In-Silico Experimental Conditions

In order to determine whether the proposed framework can reproduce the array of chromatic variations, notably associated with fluorescence emissions, observed in chlorophyll solutions exposed to multispectral light stimuli, we have incorporated it into a path tracing renderer (Section 4.2). We then employed this renderer (Appendix B) to generate

images depicting the effects of different illuminants on solutions containing distinct chlorophyll concentrations (c_{chl}). In our simulations, unless otherwise stated, we considered a quantum yield value ($Q = 0.23$) consistent with empirical data obtained for chlorophyll solutions [14].

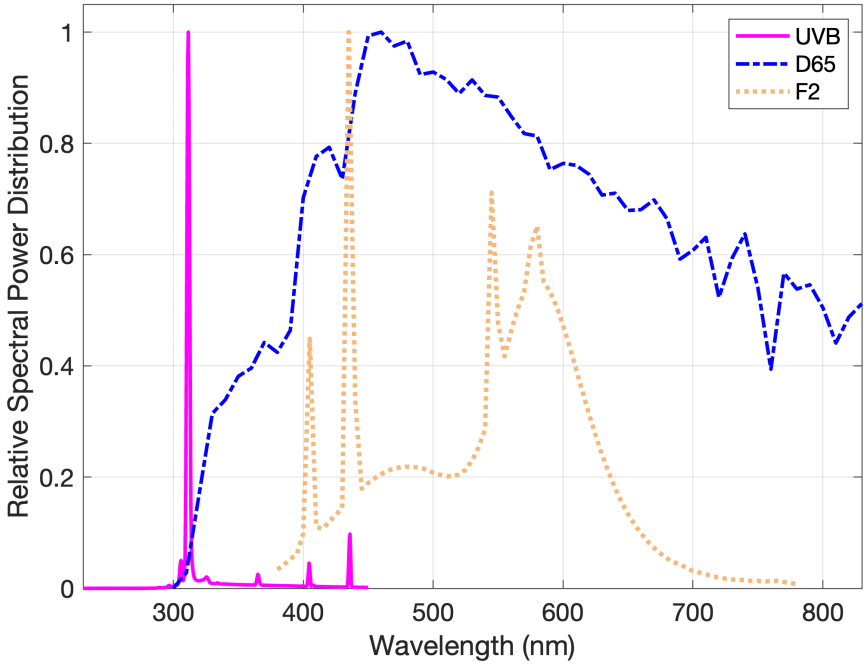

Figure 5.1: Plots of the relative spectral power distributions of the selected illuminants with stronger components in the ultraviolet (UVB [53]) and visible (D65 and F2 [7]) spectral domains.

Fig. 5.1 shows the relative spectral power distributions (RSPDs) of the selected illuminants. To increase our scope of observations, we employed light sources with strong components in spectral ranges that are commonly associated with chlorophyll fluorescence. More precisely, to represent light sources emitting primarily in the visible domain, hence-

forth referred to as visible light sources, we considered the CIE standard illuminants D65 (6,500 K, natural daylight) and F2 (fluorescent, type-2) [7], which can be used to approximate outdoor and indoor lighting conditions, respectively. On the other hand, to represent a light source emitting primarily in the ultraviolet domain, henceforth referred to as an ultraviolet light source, we utilized a UVB illuminant [53].

The molar extinction coefficient spectrum for chlorophyll employed in our simulations is provided in Fig. 5.2. It was computed using Eq. 4.9 and measured absorbance data provided by Cerovic *et al.* [9] (Fig. 2.2), which was obtained considering a concentration of 150 μM and an optical path length of 0.2 cm.

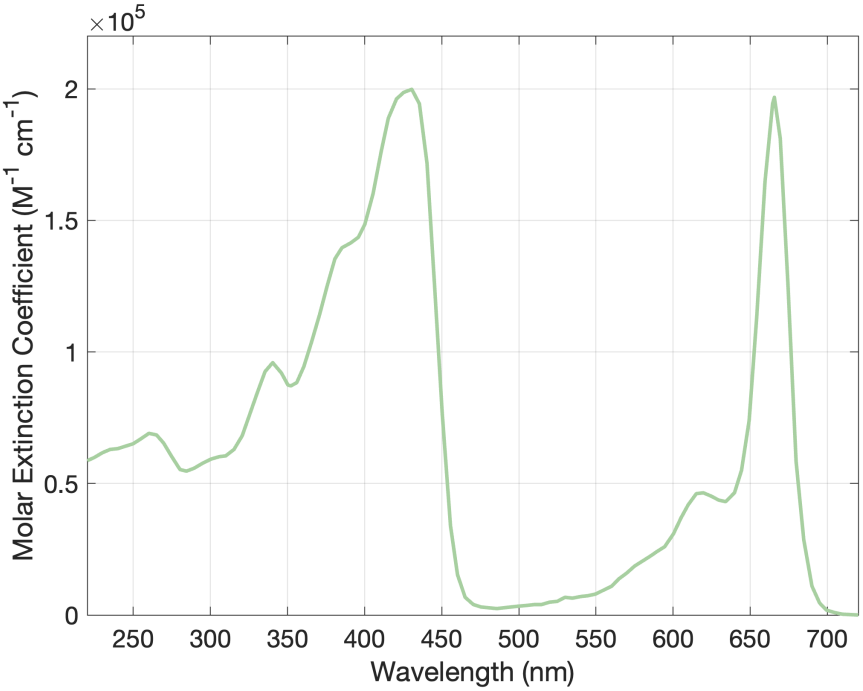

Figure 5.2: Graph depicting the molar extinction coefficient spectrum for chlorophyll employed in our simulations.

For completeness, we provide in Fig. 5.3 the chlorophyll fluorescence emission spectrum obtained using the approach described in Section 4.1.3. We note that the obtained emission spectrum shows a closer agreement with empirical chlorophyll emission data (Fig. 2.2) [9] than the Gaussian approximation (Fig. 3.1) used by previous works (Chapter 3).

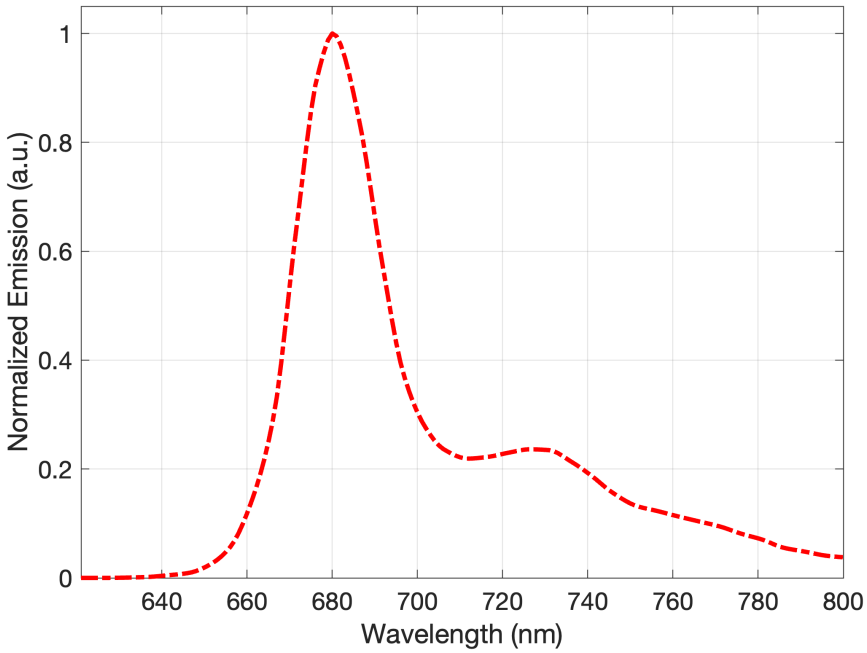

Figure 5.3: Graph depicting the chlorophyll fluorescence emission spectrum approximation derived from the *mirror-image rule* (Section 4.1.3.)

5.2 Baseline Cases

In this section, we examine the fidelity of the proposed framework's predictions with respect to fundamental qualitative aspects associated with the appearance of chlorophyll solutions under different experimental conditions. We note that, in the context of this

research, fidelity corresponds to the degree to which computer simulations can reproduce the behaviour of a real material in a perceivable manner [20].

In Fig. 5.4, we present images of chlorophyll solutions with distinct concentrations. The illuminant used in all scenes was F2 (Fig. 5.1). All solutions exhibit a green colouration, with those characterized by a higher chlorophyll concentration presenting a darker hue, which aligns with the expected light attenuation properties of chlorophyll [9]. Moreover, the fluorescence emissions are imperceptible for all solutions, which is consistent with physical observation (*e.g.*, Fig. 1.1 (top)). We remark (Chapter 2) that the fluorescence elicited by visible light is relatively weak compared to the light that is non-absorbed (*i.e.*, reflected or transmitted). Furthermore, increasing the concentration, while in theory increases the amount of fluorescence emission, does not make the emission more noticeable [69]. Thus, the images presented in Fig. 5.4 demonstrate that the modelled chlorophyll solutions under visible light exposure depict the expected appearance traits.

In Fig. 5.5, we present images of a chlorophyll solution under different visible light sources, namely the F2 and D65 illuminants (Fig. 5.1). We remark that these illuminants were chosen to mimic indoor and outdoor lighting conditions, respectively. Similar to the observations reported for the images presented in Fig. 5.4, the fluorescence emissions cannot be observed. We also note that despite the fact that the D65 illuminant emits in the ultraviolet region, the red emission remains unnoticeable. This further demonstrates that the unabsorbed visible light contributes markedly more to the observed colour of a chlorophyll solution than its fluorescence, which is tied to red emissions [24].

In Fig. 5.6, we present images illustrating the chlorophyll fluorescence emissions that can be observed when a solution is illuminated by an ultraviolet light source, namely the UVB illuminant (Fig. 5.1). The purpose of this case is two-fold. First, we show that when the light source has a dominant ultraviolet component, the fluorescence (red) emissions

Figure 5.4: Images depicting chlorophyll solutions with increasing chlorophyll concentrations. From top-left to bottom-left, clockwise: $c_{chl} = 0.02\,\mu M$, $c_{chl} = 1\,\mu M$, $c_{chl} = 5\,\mu M$ and $c_{chl} = 25\,\mu M$. For all images, the employed light source corresponds to the F2 illuminant.

Figure 5.5: Images depicting a chlorophyll solution exposed to the F2 (left) and D65 (right) illuminants. The value assigned for the chlorophyll concentration was $c_{chl} = 5\ \mu M$.

are trivially noticeable (Fig. 5.6 (right)), as expected (*e.g.*, Fig. 1.1 (middle)). Moreover, in order to isolate the fluorescence component of our proposed framework and evaluate its ability to produce plausible images, we compare a solution with $Q = 0.23$ to one with $Q = 0$. This highlights the idea that, in a hypothetical scenario where the quantum yield is equal to zero, the amount of light energy that is re-emitted is also equal to zero [39, 65]. This should, in theory, be illustrated by a solution whose appearance is given by only non-absorbed light. This matches the image presented Fig. 5.6 (left) where the only noticeable colour of the solution is the violet elicited by the non-absorbed (visible) rays. This controlled comparison is intended to verify that the emission term in our framework is correctly gated by the modifiable quantum yield parameter and responds as expected.

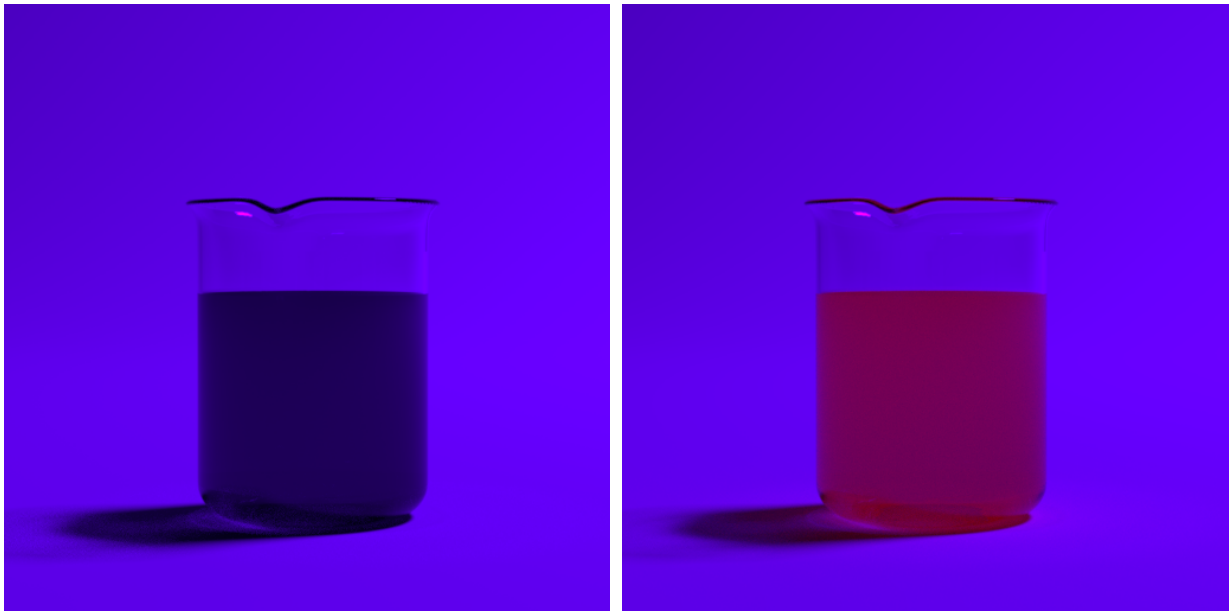

Figure 5.6: Images depicting chlorophyl solutions with the same concentration ($c_{chl} = 5\,\mu M$) and distinct quantum yields, namely $Q = 0$ (left) and $Q = 0.23$ (right), exposed to the UVB illuminant.

5.3 Extended Cases

In this section, to extend our scope of observations and further demonstrate the plausibility and robustness of the proposed framework, we examine scenarios in which the chlorophyll solutions are simultaneously illuminated by ultraviolet and visible light sources. Furthermore, we also take into account distinct light incidence geometries. To the best of our knowledge, chlorophyll fluorescence simulations and visualizations involving these illumination set-ups have not been presented in the literature to date.

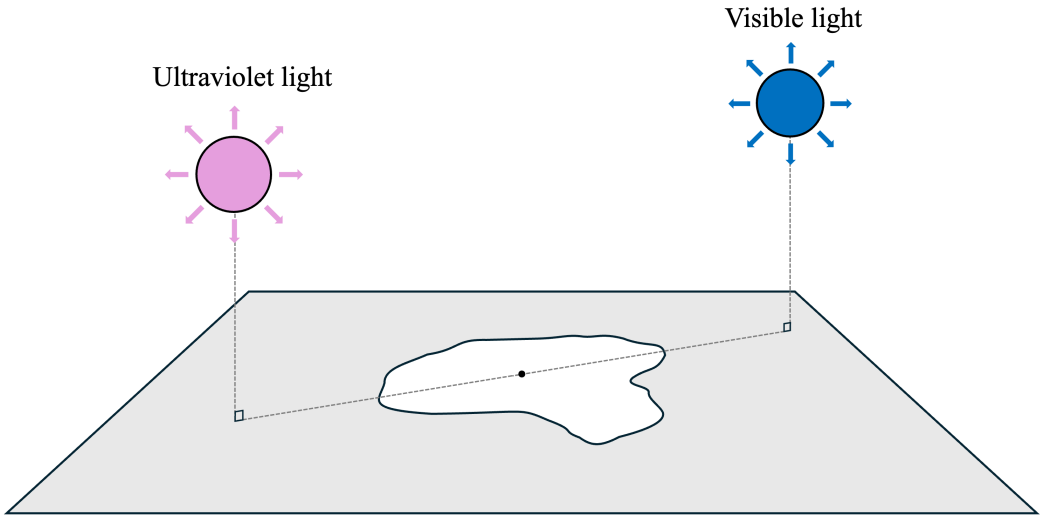

Figure 5.7: Sketch illustrating the positions of the diffuse light sources employed in the generation of the images of a chlorophyll spill presented in Fig. 5.8. The ultraviolet light source is represented by the UVB illuminant, while the visible light source is represented by the D65 illuminant.

In Fig. 5.8, we present images depicting a scenario in which a chlorophyll solution spill is exposed to ultraviolet and visible illumination (Fig. 5.7), provided by the UVB and D65 illuminants (Fig. 5.1), respectively. When the spill is exposed only to visible light, its transparent appearance presents a characteristic green hue (Fig. 5.8 (top)). On the other hand, when it is exposed to both ultraviolet and visible light, with both excitation pathways contributing roughly equally across the target surface, the resulting appearance is a mixed hue of the characteristic green of chlorophyll under visible light and the red fluorescent emission elicited by the ultraviolet light source (Fig. 5.8 (bottom)). This hue is perceived as a single colour, unlike what can be observed in the next scenario (Fig. 5.9).

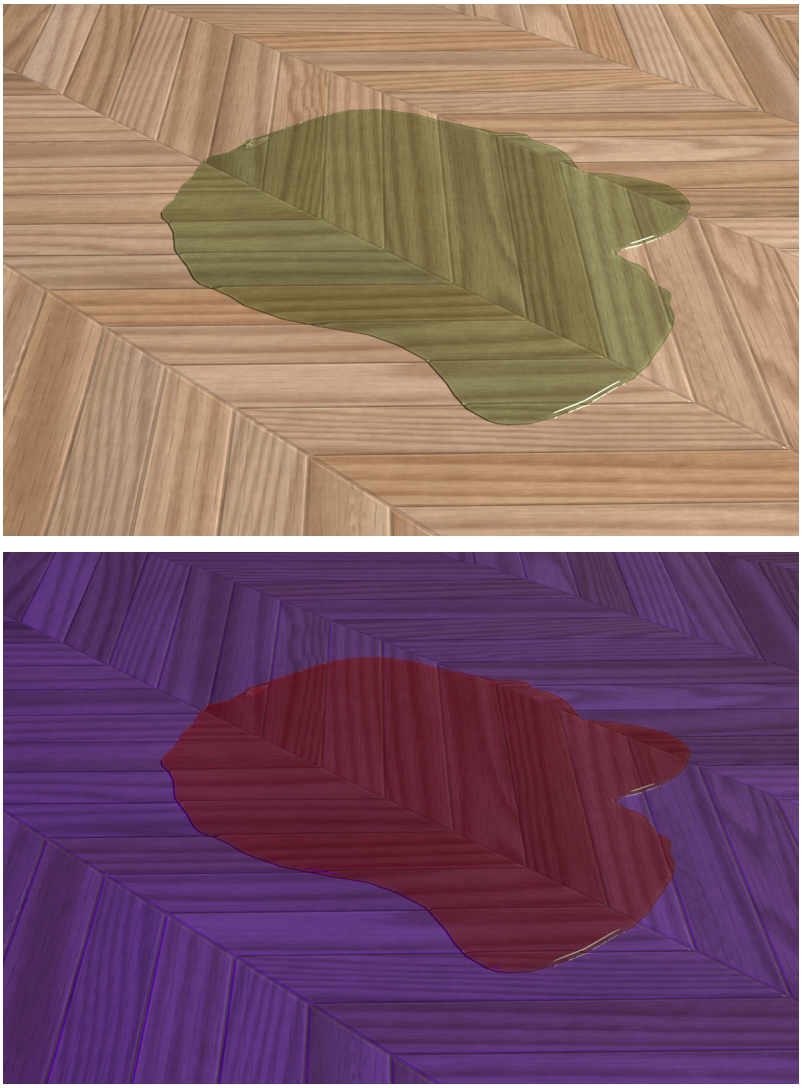

Figure 5.8: Images of a chlorophyll solution ($c_{chl} = 1\ \mu M$) spill under different illumination conditions associated with the activation of the diffuse ultraviolet and visible light sources depicted in Fig. 5.7. Top: only the visible light source is activated. Bottom: the ultraviolet and the visible light sources are both activated.

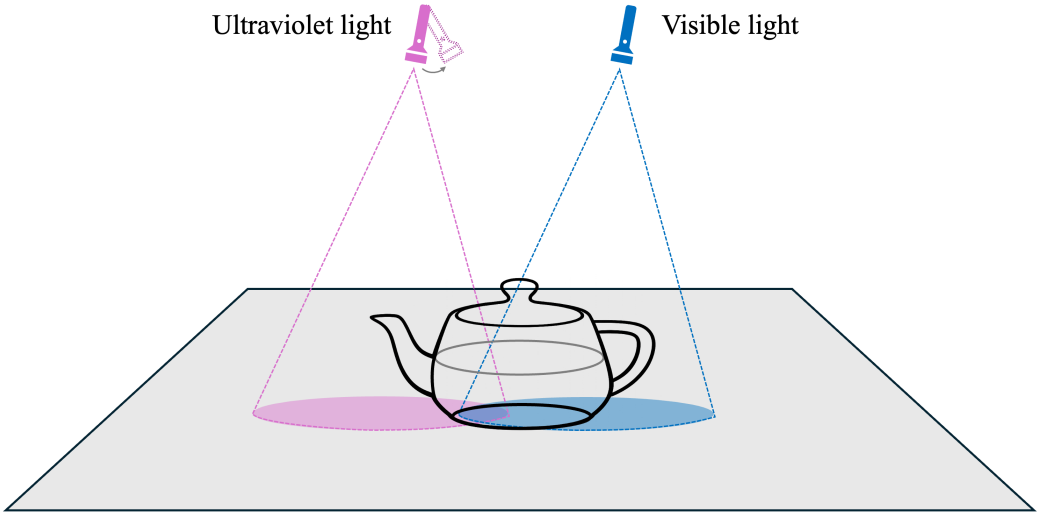

Figure 5.9: Sketch illustrating the positions of the directional light sources employed in the generation of the images of a chlorophyll-containing (transparent) teapot presented in Fig. 5.10. The ultraviolet source is represented by the UVB illuminant, while the visible light source is represented by the D65 illuminant. Note that the orientation of the ultraviolet light source is not fixed.

In Fig. 5.10, we present a sequence of images depicting a chlorophyll solution also being simultaneously exposed to directional ultraviolet and visible illumination provided by the UVB and D65 illuminants (Fig. 5.1), respectively. However, in this scenario, while the illumination area of the D65 illuminant (visible light) is kept fixed (on the right side of the teapot), the illumination area of the UVB illuminant (ultraviolet light) is not. More specifically, its target illumination area is changed (angularly, counter-clockwise) from the plane directly below it to the transparent teapot (Fig. 5.9). As a result, the chlorophyll's characteristic green from the interaction with visible light and the red fluorescence from the interaction with the ultraviolet light are depicted. Crucially, the two colours spatially coexist as observed in similar real scenarios (*e.g.*, Fig. 1.1 (bottom)). This is presumably

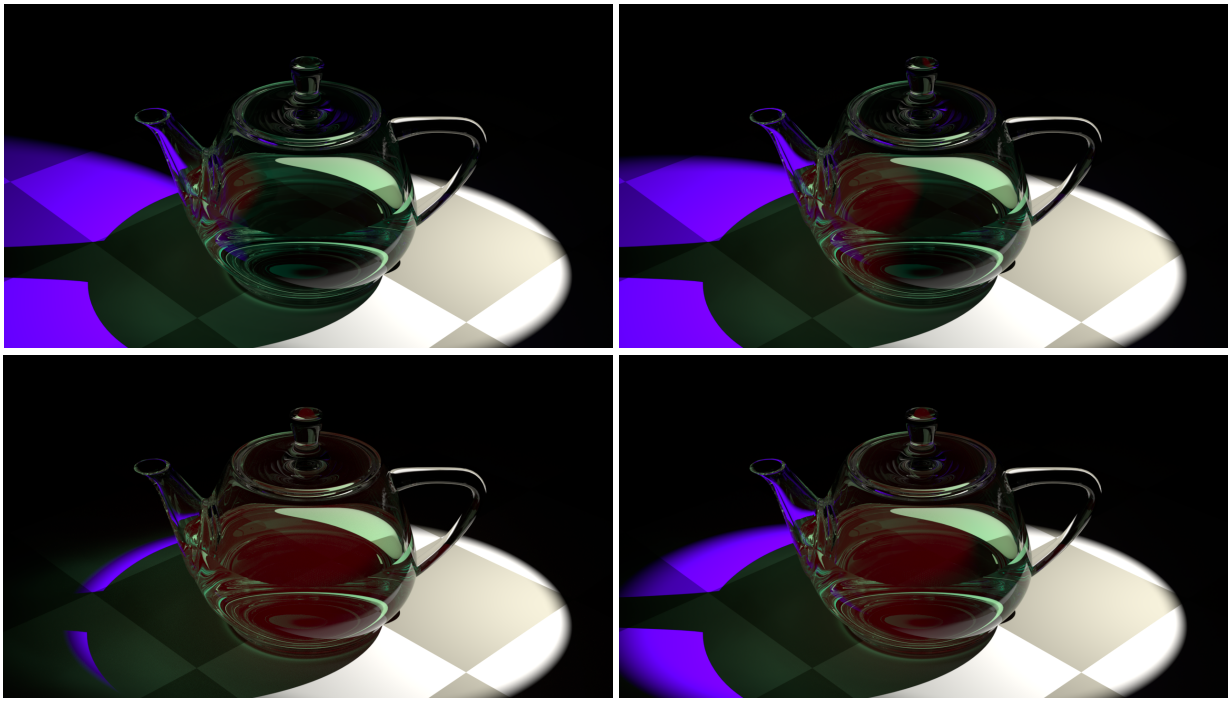

Figure 5.10: Sequence of images depicting a chlorophyll solution ($c_{chl} = 50\,\mu M$) being simultaneously illuminated by ultraviolet and visible (directional) light sources as indicated in Fig. 5.9. From top-left to bottom-left, clockwise, the images show the colour variations resulting from changing (angularly, counter-clockwise) the ultraviolet light source's target illumination area, from the plane directly below it to the transparent teapot containing the chlorophyll solution.

due to the non-uniform illumination from the two light sources, as well as the perturbation of light from the refraction caused by the glass that surrounds the medium. These aspects additionally indicate that the perceptual outcome of combined illumination is also dependent on the scene geometry, the relative orientation of the light sources and the viewer's position. The proposed framework is able to capture this nuance, which is highlighted in the comparison presented in Fig. 5.11.

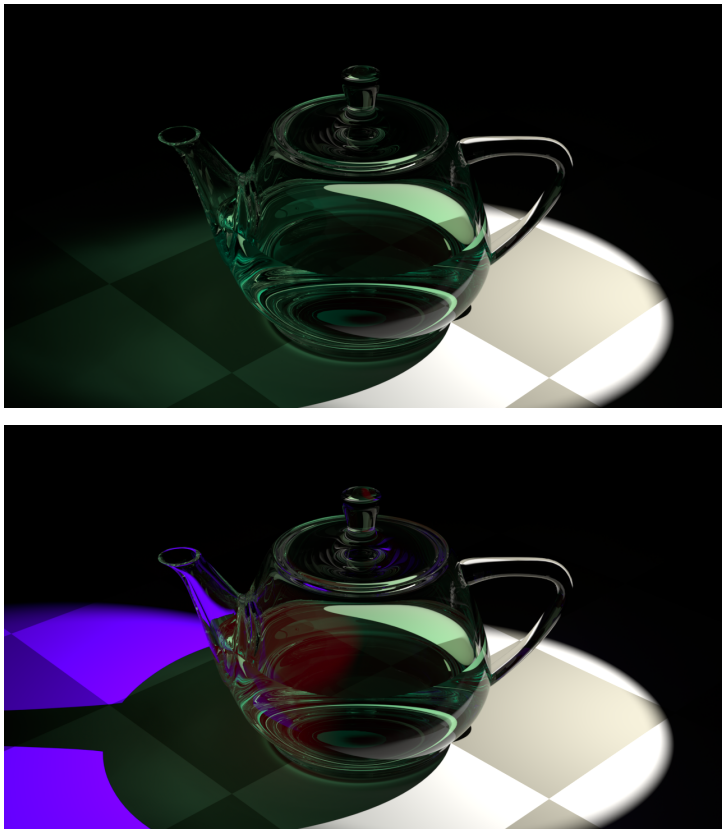

Figure 5.11: Images depicting the scenario described in Fig. 5.9 with only the visible light source activated (top) and with both, the ultraviolet and visible light sources, activated (bottom). In the latter case, the ultraviolet light source is slightly aimed at the teapot.

It is worth noting that the scenarios depicted in the images presented in this chapter are also intended to provide illustrative examples of potential applications of the proposed framework in realistic image synthesis [19]. These applications may involve objects with distinct geometries and exposed to a broader array of illumination conditions. Moreover, the described appearance changes prompted by fluorescence can be further expanded by systematically modifying the characterization parameters of target materials.

Chapter 6

Conclusion

In this thesis, we have proposed a biophysically-based framework for the multispectral simulation and visualization of chlorophyll fluorescence. Employing a stochastic algorithmic approach, it allows for different light exposure set-ups to be considered. In particular, it utilizes the *mirror-image rule* to approximate the emission spectrum of chlorophyll. This strategy not only resulted in an emission spectrum that closely approximates empirical chlorophyll data, but it can also be applied to other natural materials with similar fluorescence capabilities.

We have assessed the fidelity of the proposed framework's predictions through a systematic examination of baseline and extended test cases. The obtained images clearly depicted fundamental qualitative aspects that can be observed in real demonstrations of chlorophyll fluorescence. We remark that, to the best of our knowledge, this work represents the first initiative to visually reproduce chlorophyll fluorescence elicited by independent or simultaneous exposure to ultraviolet and visible light reported in the literature. In particular, we brought to attention two distinct appearance behaviours that arise from the simultaneous

illumination of chlorophyll by light sources with strong ultraviolet and spectral components, namely a uniform, mixed hue, as well as separated hues depicted within the same material volume.

The investigation described in this thesis can be expanded in different directions. For instance, as future work, we intend to explore the predictive visualization of fluorescence prompted by other types of chlorophyll as their appearance may be different from the classical green colour of chlorophyll *a*. Furthermore, we plan to extend the use of the proposed framework to the simulation of fluorescence elicited by living chlorophyll-containing organisms, such as plants and algae, as well as to the visualization of time-dependent, light-emission phenomena such as phosphorescence.

Besides its intended use in realistic image synthesis [19], the proposed framework can contribute to relevant interdisciplinary investigations in botany [6], ecology [40, 41], remote sensing [42, 49] and photonics [60]. For instance, it offers an *in silico* platform for the testing of hypotheses on the sensitivity of chlorophyll fluorescence to environmental changes. In particular, hypotheses connecting plant health status with variations in fluorescence signatures can potentially lead to more effective procedures for the detection of diseases affecting different types of vegetation.

Lastly, the proposed framework can also be employed to support astrobiology initiatives aimed at the visualization of ecosystems on different planets whose native vegetation may be exposed to different solar emissions [37]. Plants on these planets would likely have a different appearance [37], which, in turn, may be affected by their fluorescence responses to ultraviolet and visible light.

References

[1] M. I. Aralaguppi, C. V. Jadar, and T. M. Aminabhavi. Density, viscosity, refractive index, and speed of sound in binary mixtures of acrylonitrile with methanol, ethanol, propan-1-ol, butan-1-ol, pentan-1-ol, hexan-1-ol, heptan-1-ol, and butan-2-ol. *Journal of Chemical & Engineering Data*, 44(2):216–221, 1999.

[2] G. V. G. Baranoski and J. G. Rokne. *Light Interaction with Plants: A Computer Graphics Perspective*. Horwood Publishing, Chichester, UK, 2004.

[3] L. Belcour, A. Fichet, and P. Barla. A fluorescent material model for non-spectral editing & rendering. In *Proceedings of the ACM SIGGRAPH*, New York, NY, USA, 2025.

[4] A. Benamira and S. Pattanaik. A microfacet model for specular fluorescent surfaces and fluorescent volume rendering using quantum dots. In T. Ritschel and A. Weidlich, editors, *Eurographics Symposium on Rendering*, 2023.

[5] C. F. Bohren and D. R. Huffman. *Absorption and Scattering of Light by Small Particles*. Wiley, New York, 1998.

[6] H. R. Bolhàr-Nordenkampf and G. Öquist. Chlorophyll fluorescence as a tool in photosynthesis research. In R. C. Leegood, H. R. Bolhàr-Nordenkampf, S. P. Long, D. O.

Hall, and J. M. O. Scurlock, editors, *Photosynthesis and Production in a Changing Environment*, pages 193–206. Springer Netherlands, Dordrecht, 1993.

[7] E. C. Carter, J. Schanda, R. Hirschler, S. Jost, M. R. Luo, M. Melgosa, Y. Ohno, M. R. Pointer, D. C. Rich, F. Viénot, L. Whitehead, and J. H. Wold. Colorimetry. Technical report, CIE, 2018. CIE 015:2018, 4th edition.

[8] E. Cerezo and F. J. Seron. Rendering natural waters taking fluorescence into account. *Computer Animation and Virtual Worlds*, 15(5):471–484, 2004.

[9] Z. G. Cerovic, A. Ounis, A. Cartelat, G. Latouche, Y. Goulas, S. Meyer, and I. Moya. The use of chlorophyll fluorescence excitation spectra for the non destructive in situ assessment of uv absorbing compounds in leaves. *Plant, Cell and Environment*, 25(12):1663–1676, 2002.

[10] S. Chandrasekhar. *Radiative Transfer*. Dover Publications, New York, NY, USA, 1960.

[11] S. Chandrasekhar. Stochastic, statistical, and hydromagnetic problems in physics and astronomy. In *Stochastic, Statistical, and Hydromagnetic Problems in Physics and Astronomy*, Selected papers; v. 3, Chicago, IL, USA, 1989. University of Chicago Press.

[12] L. H. Dawson and E. O. Hulburt. The scattering of light by water. *Journal of the Optical Society of America*, 27(6):199–201, 1937.

[13] J. Dorsey, H. Rushmeier, and F. Sillion. *Digital Modeling of Material Appearance*. Morgan Kaufmann/Elsevier, MA, USA, 2007.

[14] L. S. Forster and R. Livingston. The absolute quantum yields of the fluorescence of chlorophyll solutions. *The Journal of Chemical Physics*, 20(8):1315–1320, 1952.

[15] A. S. Glassner. A model for fluorescence and phosphorescence. In G. Sakas, S. Müller, and P. Shirley, editors, *Photorealistic Rendering Techniques*, pages 60–70, Berlin, 1995. Springer.

[16] A. S. Glassner. *Principles of Digital Image Synthesis*. Morgan Kaufmann Publishers, Inc, San Francisco, CA, USA, 1995.

[17] J. C. Goedheer. Fluorescence bands and chlorophyll a forms. *Biochimica et Biophysica Acta (BBA) - Specialized Section on Biophysical Subjects*, 88(2):304–317, 1964.

[18] D. S. Goodman. General principles of geometrical optics. In M. Bass, E. W. V. Stryland, D. R. Williams, and W. L. Wolfe, editors, *Handbook of Optics (Volume I: Fundamentals, Techniques, & Design)*, pages 1.3–1.109, New York, NY, USA, 1995. Optical Society of America, McGraw-Hill, Inc. Chapter 1.

[19] D. P. Greenberg, J. Arvo, E. Lafortune, K. E. Torrance, J. A. Ferwerda, B. Walter, B. Trumbore, P. Shirley, S. Pattanaik, and S. Foo. A framework for realistic image synthesis. In *SIGGRAPH, Annual Conference Series*, pages 477–494, 1997.

[20] D. C. Gross. Report from the fidelity implementation study group. In *Simulation Interoperability Workshop, Simulation Interoperability and Standards Organization*, Orlando, FL, USA, 1999. Paper 99S-SIW-167.

[21] G. G. Guilbault. *Practical Fluorescence*. CRC Press, Boca Raton, FL, USA, 2nd edition, 2020.

[22] D. Gutierrez, A. Munoz, O. Anson, and F. J. Seron. Non-linear volume photon mapping. In Kavita Bala and Philip Dutre, editors, *Eurographics Symposium on Rendering (2005)*, 2005.

[23] D. Gutierrez, F. J. Seron, A. Munoz, and O. Anson. Visualizing underwater ocean optics. *Computer Graphics Forum*, 27(2):547–556, 2008.

[24] D. O. Hall and K. K. Rao. *Photosynthesis*. Studies in biology. Cambridge University Press, Cambridge, UK, 6th edition, 1999.

[25] J. M. Hammersley and D. C. Handscomb. *Monte Carlo Methods*. Monographs on Statistics and Applied Probability. Chapman & Hall, London, 1964.

[26] H. N. Horler and J. Barber. Principles of remote sensing of plants. In H. Smith, editor, *Plants and the Daylight Spectrum*, pages 43–64, London, UK, January 1981. Academic Press.

[27] M. B. Hullin, J. Hanika, B. Ajdin, H.-P. Seidel, J. Kautz, and H. P. A. Lensch. Acquisition and analysis of bispectral bidirectional reflectance and reradiation distribution functions. *ACM Transactions on Graphics*, 29(4), July 2010.

[28] R. S. Hunter and R. W. Harold. *The Measurement of Appearance*. John Wiley & Sons, New York, NY, USA, 1987.

[29] A. Ishimaru. *Wave Propagation and Scattering in Random Media*, volume 1. IEEE Press, New York, 2nd edition, 1978.

[30] A. Jablonski. Über den mechanismus der photolumineszenz von farbstoffphosphoren. *Zeitschrift für Physik*, 94(1-2):38–46, 1935.

[31] S. Jacquemoud and F. Baret. PROSPECT: A model of leaf optical properties spectra. *Remote Sensing of Environment*, 34(2):75–92, 1990.

[32] A. Jarabo and V. Arellano. Bidirectional rendering of vector light transport. *Computer Graphics Forum*, 37(6):96–105, 2018.

[33] H. W. Jensen. Global illumination using photon maps. In *Proceedings of the Eurographics Workshop on Rendering Techniques '96*, page 21–30, Berlin, Heidelberg, 1996. Springer-Verlag.

[34] A. Jung, J. Hanika, S. Marschner, and C. Dachsbacher. A simple diffuse fluorescent BBRRDF model. In Reinhard Klein and Holly Rushmeier, editors, *Workshop on Material Appearance Modeling*. The Eurographics Association, 2018.

[35] J. T. Kajiya. The rendering equation. *Computer Graphics*, 20(4):143–150, 1986.

[36] M. Kerker. *The Scattering of Light, and Other Electromagnetic Radiation*, volume 16 of *Physical Chemistry: A Series of Monographs*. Academic Press, New York, NY, USA, 1969.

[37] N. Y. Kiang. The color of plants on other worlds. *Scientific American*, 298(4):48–55, 2008.

[38] G. H. Krause and E. Weis. Chlorophyll fluorescence and photosynthesis: The basics. *Annual Review of Plant Physiology and Plant Molecular Biology*, 42(1):313–349, 1991.

[39] J. R. Lakowicz. *Principles of Fluorescence Spectroscopy*. Springer, New York, NY, USA, 3rd edition, 2006.

[40] H. K. Lichtenthaler, C. Buschmann, U. Rinderle, and G. Schmuck. Application of chlorophyll fluorescence in ecophysiology. *Radiation and Environmental Biophysics*, 25(4):297–308, 1986.

[41] H. K. Lichtenthaler, M. Lang, M. Sowinska, F. Heisel, and J. A. Miehe. Detection of vegetation stress via a new high resolution fluorescence imaging system. *Journal of Plant Physiology*, 148:599–612, 1996.

[42] Y. Luo, D. Xie, J. Qi, G. Yan, and X. Mu. Simulating high-resolution sun-induced chlorophyll fluorescence image of three-dimensional canopy based on photon mapping. *Remote Sensing*, 16(20):3783, 2024.

[43] D. L. MacAdam. *Color Measurement: Theme and Variations*, volume 27 of *Springer Series in Optical Cciences*. Springer-Verlag, New York, NY, USA, 1981.

[44] J. D. Mason, M. T. Cone, and E. S. Fry. Ultraviolet (250-550nm) absorption spectrum of pure water. *Applied Optics*, 55(25):7163–7172, 2016.

[45] K. Maxwell and G. N. Johnson. Chlorophyll fluorescence — a practical guide. *Journal of Experimental Botany*, 51(345):659–668, 2000.

[46] E. J. McCartney. *Optics of the Atmosphere: Scattering by Molecules and Particles*. John Wiley & Sons Inc., New York, 1976.

[47] J. R. Meyer-Arendt. *Introduction to Classical and Modern Optics*. Prentice Hall, Englewood Cliffs, NJ, USA, 4th edition, 1995.

[48] C. D. Mobley. *Light and Water: Radiative Transfer in Natural Waters*. Academic Press, San Diego, 1994.

[49] G. H. Mohammed, R. Colombo, E. M. Middleton, U. Rascher, C. van der Tol, L. Nedbal, Y. Goulas, O. Pérez-Priego, A. Damm, M. Meroni, J. Joiner, S. Cogliati, W. Verhoef, Z. Malenovský, J.-P. Gastellu-Etchegorry, J. R. Miller, L. Guanter, J. Moreno, I. Moya, J. A. Berry, C. Frankenberg, and P. J. Zarco-Tejada. Remote sensing of solar-induced chlorophyll fluorescence (SIF) in vegetation: 50 years of progress. *Remote Sensing of Environment*, 231:111–177, 2019.

[50] M. Mojzík, A. Fichet, and A. Wilkie. Handling fluorescence in a uni-directional spectral path tracer. *Computer Graphics Forum*, 37:77–94, 07 2018.

[51] N. Nelson and C. F. Yocum. Structure and function of photosystems I and II. *Annual Review of Plant Biology*, 57(1):521–565, 2006.

[52] OECD (Organisation for Economic Co-operation and Development). *Test No. 101: UV-VIS Absorption Spectra*. OECD Guidelines for the Testing of Chemicals, Section 1. OECD Publishing, Paris, France, 1981.

[53] M. Paravia. Spectra of UV lamps and UV leds. Opsytec Dr. Gröbel GmbH, Ettlingen, Germany, 2026. https://www.opsytec.com/uv-applications-knowledge/spectral-database-for-uv-lamps-and-uv-leds.

[54] G. D. Parfitt and J. A. Wood. Rayleigh ratios of pure liquids; comparison of experiment with theory. *Transactions of the Faraday Society*, 64:805–814, 1968.

[55] M. Pharr, W. Jakob, and G. Humphreys. *Physically Based Rendering: From Theory to Implementation*. MIT Press, Cambridge, MA, USA, 2023.

[56] E. R. Pike, W. R. M. Pomeroy, and J. M. Vaughan. Measurement of rayleigh ratio for several pure liquids using a laser and monitored photon counting. *The Journal of Chemical Physics*, 62(8):3188–3192, 1975.

[57] R. M. Pope and E. S. Fry. Absorption spectrum (380–700 nm) of pure water. II. integrating cavity measurements. *Applied Optics*, 36(33):8710–8723, 1997.

[58] S. A. Prahl. *Light Transport in Tissue*. PhD thesis, The University of Texas at Austin, USA, December 1988.

[59] E. I. Rabinowitch. *Light absorption by pigments in the living cell*, volume 2, chapter 51, pages 672–739. Interscience Publishers, Inc., 1951. Part 1.

[60] G. S. Senesi, O. De Pascale, B. S. Marangoni, A. R. L. Caires, G. Nicolodelli, V. Pantaleo, and P. Leonetti. Chlorophyll fluorescence imaging (CFI) and laser-induced breakdown spectroscopy (LIBS) applied to investigate tomato plants infected by the root knot nematode (RKN) meloidogyne incognita and tobacco plants infected by cymbidium ringspot virus. *Photonics*, 9(9), 2022.

[61] P. Shirley. *Physically Based Lighting for Computer Graphics*. PhD thesis, Dept. of Computer Science, University of Illinois, USA, January 1991.

[62] M. Smoluchowski. Molecular-kinetic theory of the opalescence of gases in a critical state, as well as several related occurrences. *Annalen der Physik*, 25(2):205–226, 1908.

[63] G. G. Stokes. On the composition and resolution of streams of polarized light from different sources. *Transactions of the Cambridge Philosophical Society*, 9:399, 1851.

[64] G. G. Stokes. On the change of refrangibility of light. *Philosophical Transactions of the Royal Society of London*, 142:463–562, 1852.

[65] B. Valeur and M. N. Berberan-Santos. *Molecular Fluorescence: Principles and Applications*. Wiley-VCH, Weinheim, Germany, 2nd edition, 2012.

[66] R. A. Velapoldi and K. D. Mielenz. Standard reference materials: A fluorescence standard reference material: Quinine sulfate dihydrate, 1980.

[67] L. P. Vernon and G. R. Seely. *The Chlorophylls*. Academic Press, New York, NY, USA, 1966.

[68] T. C. Vogelmann, C. Critchley, and W. K. Smith. *Photosynthetic Adaptation: Chloroplast to Landscape*, volume 178 of *Ecological Studies*. Springer, New York, 1st edition, 2004.

[69] W. F. Watson and R. Livingston. Self-quenching and sensitization of fluorescence of chlorophyll solutions. *The Journal of Chemical Physics*, 18(6):802–809, 1950.

[70] A. Wilkie, R. F. Tobler, and W. Purgathofer. Combined rendering of polarization and fluorescence effects. In S. J. Gortler and K. Myszkowski, editors, *Rendering Techniques 2001*, pages 197–204, Vienna, Austria, 2001. Springer.

APPENDICES

Appendix A

Chlorophyll: From Chloroplasts to Photosynthesis

In this appendix, we provide a brief overview of the process of photosynthesis and how fluorescence occurs as a byproduct. Through photosynthesis, plants use the absorbed energy from inorganic compounds and solar radiation in order to synthesize food materials and other organic compounds [24, 68]. These compounds, in turn, have a vital importance for most of the lifeforms on Earth.

This fundamental process is facilitated by chloroplasts, specialized organelles located within plant cells [68]. Each chloroplast organelle contains many thylakoids, a disc-like compartment which houses the photosynthetic apparatus in its membrane [24]. The photosynthetic apparatus of a photosynthetic organism (*e.g.*, leaves, algae, phototrophic bacteria) is a system of protein-pigment complexes and molecules. Included in these protein-pigment complexes is chlorophyll, the pigment responsible for absorbing light and converting the absorbed energy into fuel for photochemical and enzymatic reactions [24]. Also, the typical

Figure A.1: The effects of chlorophyll on foliar appearance. Left: photograph depicting the reflection and transmission of sunlight onto leaves. Right: microscope photograph showing the internal layers of a plant leaf laden with chlorophyll-containing chloroplasts.

green colour of algae and plants (Fig. A.1) are prompted by the specific light absorption profiles of chlorophyll, with mainly blue and red light being absorbed, while green light is propagated (reflected or transmitted) [2, 9].

The energy absorbed is then transferred to the reaction centers of two photosystems, namely the Photosystem I (PSI) and Photosystem II (PSII) located in the thylakoid membrane, leading to electron excitation [38]. These photosystems convert the excited energy to catalyze the production of oxygen and the assimilation of carbon dioxide within the chloroplast [51]. Excess excited energy is dissipated and it may be released in the form of heat or light. In the latter case, the light emissions can bring about the visual manifestation of *fluorescence*, the focal point of the research described in this thesis. It is worth noting that maximum quantum yield of chlorophyll *a* observed under *in vivo* conditions (*e.g.*, from a plant leaf or an alga) is around eight to ten times lower than that observed under *in vitro* conditions (*e.g.*, from a solution) [14, 38].

Appendix B

Integration of Fluorescence into a Path Tracing Renderer

The proposed framework was implemented in the `pbrt-v4` renderer [55]. More specifically, it was implemented as a new medium class, `ChlorophyllMedium`. The majority of the logic is coded within the `VolPathIntegrator::Li()` function and extends the existing volumetric path tracing infrastructure to handle fluorescence events that occur in a `ChlorophyllMedium`.

When a camera ray enters a `ChlorophyllMedium` region, a transmittance value, `T_reg`, is sampled via Eqs. 4.3, 4.4, and 4.5. If the sampled path length, p_i exceeds the distance to the volume boundary, d_1, the camera ray is deemed to have not interacted with a `ChlorophyllMedium` particle and is transmitted. Otherwise, the camera ray is determined to be attenuated. The attenuation event is stochastically determined to be either a scattering or absorption event. Their respective probabilities are given by Eq. 4.2 and Eq. 4.1. If the ray is scattered, its perturbed direction is determined via the Rayleigh scattering

distribution [46] (Algorithm 1). The ray continues to be traced by `pbrt-v4`, outside of our additional code. If the ray is absorbed, the integrator[1] checks whether the ray's wavelength lies within the domain of the emission spectrum, which is obtained via Section. 4.1.3. If so, then, if a sampled uniform random number is less than Q, the camera ray is deemed to be a fluoresced ray. Otherwise, the ray is terminated and we stop tracing the path.

Proceeding with the fluoresced ray, a light source is sampled using the `LightSampler()` function and a point on its surface is sampled via the renderer's `SampleLi()` function. An excitation wavelength λ_e is sampled uniformly within the intersection of the light source's spectral power distribution and the range of wavelengths shorter than the camera ray's wavelength. A shadow ray[2] is spawned from the attenuation point towards the sampled position on the light source. The shadow ray's transmittance through the medium at the excitation wavelength is sampled, again using Eqs. 4.3, 4.4, and 4.5. If an opaque surface intersection is detected along the shadow ray, the contribution is set to zero and the path is terminated. If the sampled path length p_e is less than the distance d_2 from the attenuation point to the volume boundary, we stop tracing the ray and terminate it. Otherwise, we continue tracing it.

The fluorescence contribution of the path is added to the radiance estimate L. This contribution is calculated by multiplying the sampled light source radiance by a number of scalars. These scalars consist of the following terms: the path throughput weight (which

[1] An integrator is the top-level rendering algorithm responsible for estimating the radiance along each camera ray by numerically solving the rendering equation, typically via Monte Carlo sampling [35].

[2] We borrow the term *shadow ray* from the path tracing literature [61], where it refers to a ray cast from an interaction point toward a light source to evaluate the direct illumination contribution. In our framework, *the shadow ray* serves the same structural purpose by connecting the fluorescence interaction point to the sampled light source, albeit carrying the sample excitation wavelength rather than the camera ray's wavelength.

encapsulates the accumulated transmittance and PDF[3] factors along the camera ray), the transmittance from the ray's entry point to the interaction point, the shadow ray transmittance, and the normalized emission spectrum. The product of the aforementioned scalars is then divided by the channel[4] average of the rescaled path probability — maintained by the integrator as part of `pbrt-v4`'s spectral multiple importance sampling procedure — and the light sampling probability normalized by the first channel's value. After calculating the ray's contribution as indicated above, we stop tracing it.

[3]A probability density function (PDF) describes the likelihood of a continuous random variable taking on a given value [25]. In rendering, it characterizes the probability of sampling a particular direction, position, or wavelength during Monte Carlo integration [35].

[4]In `pbrt-v4`, each ray carries N simultaneously sampled wavelengths, and all spectral quantities are represented as `SampledSpectrum` values containing one component per carried wavelength. The first wavelength, at index 0 (*i.e.*, the first channel), is sampled uniformly over the visible range (unless another range is specified) and determines all directional sampling decisions. The remaining wavelengths are placed at equal bins to ensure uniform spectral coverage. In our implementation, we set $N = 12$.

Index